Catalysis Today 468 (2026) 115740

Contents lists available at ScienceDirect

Catalysis Today

journal homepage: www.elsevier.com/locate/cattod

Investigating the photoactivity of Cu_2O-TiO_2 (Home Prepared) composites for H_2 production by photoreforming under natural solar light in a pilot plant photoreactor

Muhammad Umair [a], Alba Ruiz-Aguirre [b], Ilaria Berruti [b], Leonardo Palmisano [a], Sixto Malato Rodríguez [b,*], Vittorio Loddo [a], Marianna Bellardita [a,*]

[a] Engineering Department, University of Palermo, Viale delle Scienze Ed. 6, Palermo 90128, Italy
[b] CIEMAT – Plataforma Solar de Almería, Ctra. DeSenés s/n, Tabernas, Almería 04200, Spain

ARTICLE INFO

Keywords:
Photocatalysis
Semiconductor composites
Glucose
Ethanol
Glycerol
Solar photo-reactor

ABSTRACT

Home-prepared TiO_2 containing an anatase/rutile mixture was coupled with different Cu_2O amounts by the ball milling method technique. The samples were characterized by UV-Vis diffuse spectroscopy (DRS), specific surface area (SSA) determination, photoluminescence (PL) and Raman spectra, X-ray diffraction (XRD), scanning electron microscopy (SEM), transmission electron microscopy (TEM), X-ray photoelectron spectroscopy (XPS), Electron Paramagnetic Resonance (EPR) and photoelectrochemical measurements. The photocatalytic activity was studied for H_2 production under natural solar light irradiation in a pilot plant reactor in the presence of different sacrificial agents. An effective heterojunction that enhanced the charge transfer processes, was formed between the components, as confirmed by photoluminescence spectra. 3 %Cu_2O-TiO_2 was the most active photocatalyst and the presence of Cu_2O (instead of the noble metals generally used) was efficient for H_2 production with 62 mmol obtained after 5 h (equivalent to ca. 5 mmol g^{-1} h^{-1}) of solar irradiation starting from glycerol, which yielded the highest H_2 amount with respect to the other sacrificial agents. Copper was present in different oxidation states and a moderate amount of leaching of Cu species was found. Holes, $OH^{\bullet}$ and $O_2^{\bullet-}$ radicals were the main active species for glycerol degradation, while a higher availability of photoproduced electrons was beneficial for H_2 production.

1. Introduction

Growing energy demand driven by population and industrial expansion has long relied on fossil fuels, but their associated CO_2 and greenhouse-gas emissions make them incompatible with current climate-neutrality goals, such as those outlined in the European Green Deal [1–4]. Hydrogen is an attractive clean fuel due to its high energy density and water as its only combustion product [5], yet conventional production methods are energy-intensive and carbon-emitting [6]. This motivates the search for greener alternatives. Solar energy offers a renewable and abundant resource that can be converted into chemical fuels [7]. In this context, the photoreforming of organic compounds emerges as a sustainable route for CO_2-free H_2 generation [8,9], especially when using biomass-derived substrates [10], which are renewable and carbon-neutral. The most common sacrificial compounds are alcohols, such as glycerol, ethanol and methanol, as well as formic acid and sugars. Ethanol, which is produced from low-grade biomass and sewage sludge, provides a sustainable and economical route to produce H_2 through its photoreforming [11]. Formic acid, which contains 4.4 % (w/w) hydrogen is a cheap, non-flammable, non-toxic and highly stable compound, and is considered very suitable because it decomposes directly into H_2 and CO_2 by a thermodynamically favourable reaction [12,13]. However, its use as a hole trap is neither advisable nor cost-effective, since for every two grams of H_2, 44 g of CO_2 are simultaneously emitted. Furthermore, formic acid can be considered a valuable compound, used as an intermediate in chemical synthesis and other applications, such as in the paper, pharmaceutical, and textile industries. A particularly interesting molecule for the production of high value chemicals and H_2 is glycerol which is derived from cellulose and starch [14,15]. It represents about 10 % of the volume of biodiesel industries [16], and with the increase in biodiesel production, crude oil disposal is becoming a serious problem [17]. Photocatalytic technology

* Corresponding authors.
E-mail addresses: smalato@psa.es (S.M. Rodríguez), marianna.bellardita@unipa.it (M. Bellardita).

https://doi.org/10.1016/j.cattod.2026.115740
Received 28 November 2025; Received in revised form 9 February 2026; Accepted 17 February 2026
Available online 17 February 2026

represents a promising, environmentally friendly method not only to obtain H_2 from glycerol, but also to convert it into valuable chemicals [18,19].

Although TiO_2 is the most investigated photocatalyst [20], it has many weaknesses to overcome [21]. Various strategies aimed at enhancing the visible light absorption, increasing the surface area, and improving the charge transfer processes, have been investigated to improve its performance [22−24], with particular attention to H_2 production [25]. Loading TiO_2 surface with noble metals is very effective in increasing photocatalytic H_2 production [26,27]. However, for practical applications, this option is limited due to the high cost of noble metals. Combining TiO_2 with another semiconductor is a successful strategy to inhibit the hole–electron pairs recombination [28−32]; notably, choosing semiconductors with appropriate conduction and valence band energy levels, H^+ reduction to H_2 is thermodynamically favourable [33−35].

TiO_2 exists in three main polymorphs, i.e. anatase, brookite, and rutile, displaying different energy levels of their valence and conduction bands [36]. It has been shown that the simultaneous presence of multiple TiO_2 phases allows the formation of a heterojunction that has the same behaviour as that obtained coupling different semiconductors [32, 36−38]. This is one of the features that explains the high photocatalytic activity of Degussa P25, the most widely used commercial TiO_2 [39,40]. It should be remembered, however, that in addition to the phase composition of TiO_2-based photocatalysts, many other parameters such as the presence of defects, the degree of surface hydroxylation and acidity and basicity, influence their photoactivity [41]. For this reason, there is a continuous effort by researchers in the preparation of photocatalysts with tailored synthesis conditions.

As an alternative to noble metals, Cu_2O is a p-type semiconductor with a narrow band gap (2.0–2.2 eV), low cost, low toxicity, and suitable bands energy levels, which, coupled with TiO_2, has proven to be effective in producing H_2 via photoreforming [42,43]. Plascencia-Hernández et al. [42] prepared Cu_xO/TiO_2 (P25) composites via chemical reduction using different amounts of copper chloride. Characterization techniques revealed that, during the photocatalytic reforming of methanol under simulated solar light, Cu was present in different forms (CuO, Cu_2O, and Cu^0). The best results were obtained by loading small amounts of Cu_xO (0.05 %w) on TiO_2, affording an H_2 evolution rate of 2.86 mmol g^{-1} h^{-1}. The coexistence of the Cu species and TiO_2 facilitated the effective separation of photogenerated charges, endorsing the photoreduction of protons. Rajendran et al. [44] tested Cu_xO/TiO_2 photocatalysts with Cu in +1 and/or +2 oxidation state for H_2 generation under sunlight irradiation using a 25 % v/v methanol/water mixture. Samples in which Cu is exclusively present in +1 oxidation state exhibited the highest H_2 production rate of 7.06 mmol h^{-1} g^{-1}. A p-n type heterojunction formed at the interface of Cu_2O-TiO_2 improved charge carrier separation and absorbance in the visible spectrum leading to high photocatalytic activity for glycerol photoreforming with an H_2 production of about 4.7 mmol g^{-1} in 24 h of irradiation with a 400 W metal halide lamp [45]. Cu_2O/TiO_2 (P25) composites obtained by a hydrothermal method showed good activity for H_2 production (evolution rate 2.55 mmol g^{-1} h^{-1}) from aqueous methanol solution under simulated sunlight irradiation in lab-scale reactors [46].

For the preparation of Cu_2O-TiO_2, to date different strategies have been used, but each is associated with some limitations, such as high reagent cost, and high operating temperature and pressure conditions. Ball milling is a simple, inexpensive, reproducible, and eco-friendly method [18,47,48] that allows the preparation of high catalysts amount in a single step.

In the present study, anatase-rutile TiO_2 was synthesized with a high specific surface area and then coupled with different percentages of Cu_2O, through the ball milling method. Photoreforming of different sacrificial agents, such as formic acid, ethanol, glucose and glycerol, was performed to generate H_2 in a pilot plant photo-reactor under natural sunlight irradiation. Formic acid and ethanol were used only for comparison and to better understand the reaction mechanism because they themselves are useful chemicals and their oxidation does not produce high-value compounds, but rather CO_2 and H_2O. Mechanistic studies were conducted to identify the main active species affecting the photocatalysts' performance. Future efforts will be focused on improving the catalyst optimized here to obtain samples to be used in pilot-scale reactors.

With respect to a previous work [49] in which CuO-TiO_2 (P25) samples were prepared by a calcination method, in the present work, commercial Cu_2O has been coupled with home-made TiO_2 by ball milling at ambient conditions.

2. Experimental

See Supporting Information.

3. Results and discussions

3.1. Characterizations

Fig. 1A shows the UV-Vis DRS spectra of the samples used. Cu_2O displays absorbance only in the visible range, while HP TiO_2 powder shows a transition edge at ca. 340 nm and a significant light absorption in the range 400–650 nm, ascribable to the presence of oxygen vacancies as can be inferred from the spectrum shape in accordance with the literature [50,51]. In the composite samples, a gradual increase in absorbance at wavelengths higher than 400 nm and a second absorption edge associated with Cu_2O can be noticed by increasing its amount from 1 % to 5 %. The band gap of home prepared TiO_2 is 3.03 eV (Table 1), that of Cu_2O 1.97 eV, and in the composites the addition of Cu_2O to TiO_2 does not alter the band gap, but two transitions can be noticed. The first one at lower wavelength is coincident with that of the hosting oxide, the second one is ascribable to Cu_2O. The presence of the two edges suggests the formation of a heterostructure between the two oxides [18,52]. In Table 1 the SSA values of the samples used are reported. The surface area of bare TiO_2 is 78 m^2 g^{-1}, that of Cu_2O 1 m^2 g^{-1} and its addition to TiO_2 causes only a small decrease in SSA due to the low Cu_2O amount and mild preparation conditions of the heterostructures.

In Fig. 1B the photoluminescence spectra of selected samples are shown. The photocatalysts exhibit two main emission peaks: the one at ca. 420 nm comes from the band-to-band emission caused by the recombination of photogenerated charges, while the peaks at higher wavelengths can be attributed to the recombination of photo-promoted electrons into defects due to oxygen vacancies [53]. The coupling of TiO_2 with 3 % and 5 % Cu_2O causes a reduction in the photoluminescence intensity due to a decrease in the recombination rate of photogenerated charges [54], while no significant changes can be observed for 1 %Cu_2O. This result can probably be explained by simply considering that the amount of hosted oxide is lower. Notably, the 3 % Cu_2O-TiO_2 sample exhibits the lowest intensity indicating an optimal charge transfer rate that can be associated with high photocatalytic activity.

The different conduction energy levels and valence band edges for TiO_2 and Cu_2O led to interfacial charge transfer, decreasing the e^-/h^+ recombination rate.

Fig. 2A reports the XRD diffractograms of the TiO_2 HP and 3 % Cu_2O-TiO_2 HP samples. The first sample consists of a mixture of anatase (main peak at $2\theta = 25.28°$) and rutile (main peak at $2\theta = 27.53°$) phases. After the addition of Cu_2O, two peaks at $2\theta = 36.5°$ and 42.4 ° were also recorded, corresponding to the (111) and (200) crystal planes of Cu_2O, respectively, in agreement with the literature [55].

The relative amount of anatase and rutile, contained in the crystalline part of TiO_2, was determined by the following equations [56]:

$$W_A = \frac{0.886 \cdot A_A}{0.886 \cdot A_A + A_R}$$

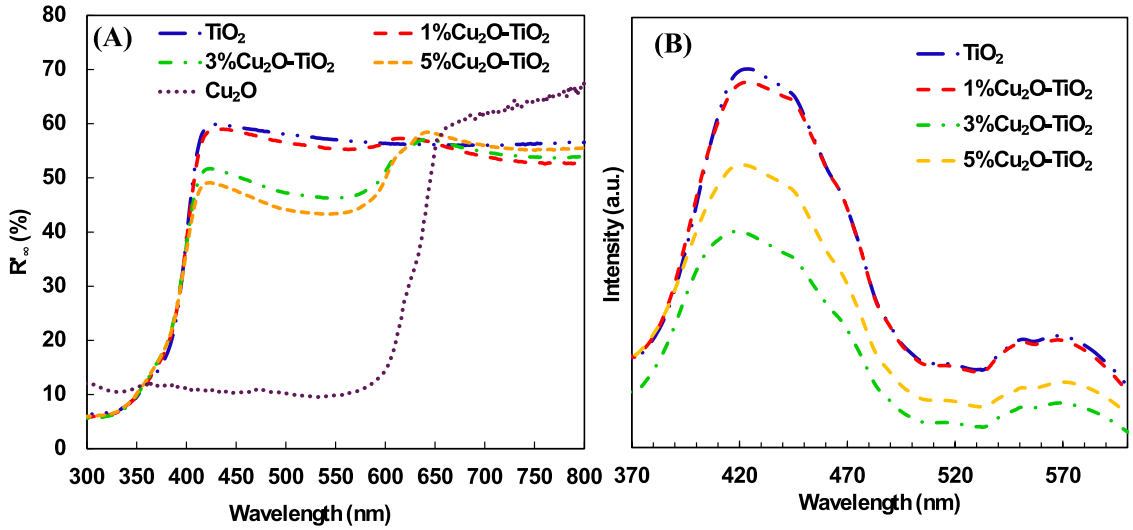

Fig. 1. UV-Vis DRS (A) and photoluminescence (B) spectra of the used samples.

Table 1
Band gap and SSA values of the used photocatalysts.

Samples	Band gap (eV)	SSA ($m^2\ g^{-1}$)
TiO_2 HP	3.03	78
1 %Cu_2O-TiO_2 HP	3.02	72
3 %Cu_2O-TiO_2 HP	3.02	69
5 %Cu_2O-TiO_2 HP	3.03	68
Cu_2O	1.97	1

$$W_R = \frac{A_R}{0.886 \cdot A_A + A_R}$$

In which A_A and A_R represent the integrated intensity of the anatase peak at $2\theta = 25.3^\circ$ and of the rutile one at $2\theta = 27.5^\circ$, respectively. Bare TiO_2 HP consisted of ca. **77.5 %** of anatase and 22.5 % of rutile exhibiting a phase composition very similar to that of TiO_2 P25. After the ball milling treatment in the presence of 3 % Cu_2O, the relative amounts of anatase and rutile were 83 and 17 %, respectively. An explanation can be found in the fact that, during ball milling, a crystallization of part of the amorphous phase into the anatase phase occurred, and in support of this hypothesis it should be noted that the peaks in the diffractogram of 3 %Cu_2O-TiO_2 HP are narrower and more intense than those of the starting pure TiO_2.

In Fig. 2B the Raman spectra of bare TiO_2 HP and its composite with 3 % Cu_2O are reported. In the TiO_2 sample, only the characteristic anatase bands at 144 cm^{-1}, 197 cm^{-1}, 396 cm^{-1}, 514 cm^{-1} and 637 cm^{-1} are visible, whilst no band attributable to rutile is present due to its lower content with respect to anatase. In 3 %Cu_2O-TiO_2 HP no peaks of Cu_2O are visible, probably due to the low amount and high degree of dispersion on TiO_2 surface. However, by enlarging the main anatase peak associated with the O-Ti-O vibration (inset of Fig. 1B), a slight red shift, attributable to a bond distortion into the TiO_2 lattice, can be noticed [57]. This finding confirms an interaction between TiO_2 and Cu_2O in the composite samples.

Fig. 3 (A,B) shows the SEM images of TiO_2 HP and 3 %Cu_2O-TiO_2 HP powders. Irregular rounded-shaped aggregates with sizes ranging from 20 to 130 nm can be observed in TiO_2 HP, without changes in morphology after the addition of Cu_2O, probably due to the relatively small amount of Cu_2O compared to TiO_2 and uniform mixing. The morphology of the powder recovered after photocatalytic tests (Fig. 3C) is substantially the same as that of the "fresh" sample, indicating that the photocatalyst is stable to the mechanical stresses due to mixing in water. TEM images were also acquired to study the distribution of components and particles dimensions. In Fig. 3 (D), Cu_2O showed particle size ranges between 5 and 10 nm, while sizes of TiO_2 HP particles were between 5

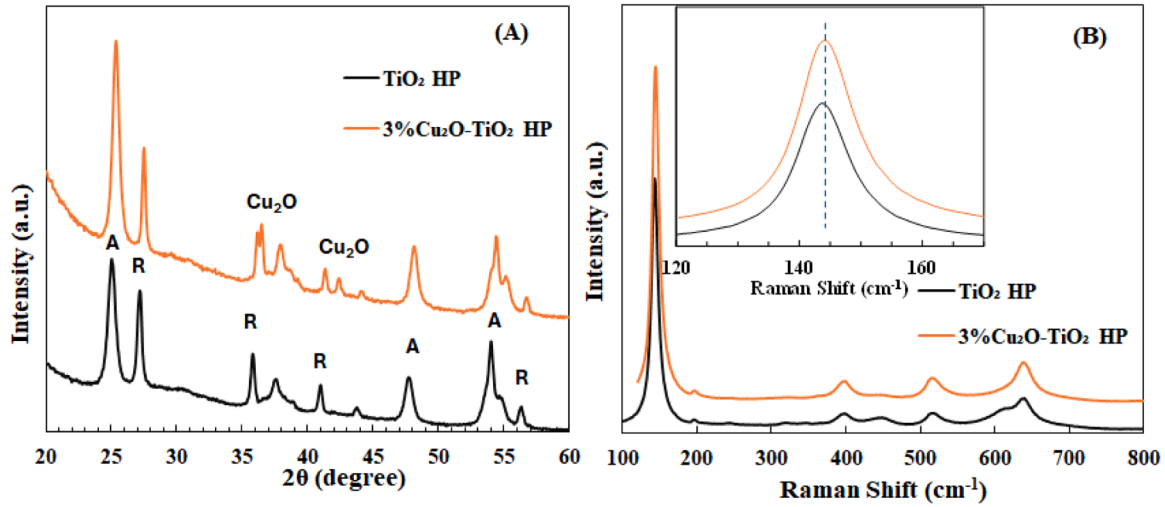

Fig. 2. XRD patterns (A) and Raman spectra (B) of TiO_2 HP and 3 %Cu_2O-TiO_2 HP.

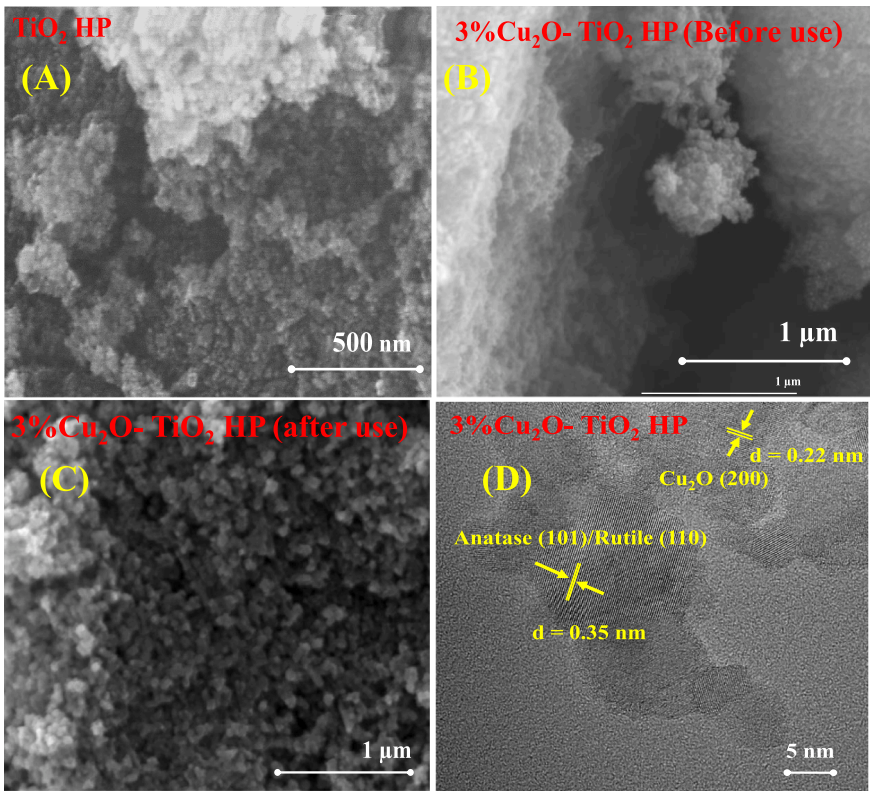

Fig. 3. SEM images of TiO_2 HP (A), 3 %Cu_2O-TiO_2 HP before (B) and after the photocatalytic tests (C) and TEM image of 3 %Cu_2O-TiO_2 HP (D).

and 25 nm. The lattice fringes of ca. 0.35 nm can be attributed both to the (101) plane (d= 0.352 nm) of anatase TiO_2 or to the (110) (d= 0.324 nm) of rutile TiO_2 (due to the small difference between the two values and the relative low content of rutile) [58,59], while the lattice fringes of Cu_2O (200) planes are ca. 0.22 nm [60].

Fig. 4A shows the XPS binding energy peaks characteristic of Ti 2p, O 1 s and Cu 2p species present in bare TiO_2 and in the 3 %Cu_2O-TiO_2 samples. Peaks identified in bare TiO_2 at binding energies 459.1 eV and 464.9 eV are representative of Ti 2p3/2 and Ti 2p1/2 transitions, respectively. The presence of these two peaks, with a binding energy separation of 5.8 eV, indicates that Ti is present mainly in the + 4 oxidation state [61]. The minor signal at 470 eV (better visible in the deconvolution of the spectrum (Fig. 4B)) is reported as a shake-up satellite band reflecting weak background effects or subtle surface species that does not significantly alter the assignment of Ti^{4+} in TiO_2 [62]. In the 3 %Cu_2O-TiO_2 HP composite the Ti 2p peaks display a little shift towards lower binding energies, and this behaviour can be ascribed to the formation of surface Ti^{3+} species, probably due to some degree of oxidation of Cu^+ to Cu^{2+} [63,64]. For both samples, the O 1 s spectra have a main peak at 530.7 eV (see Figs. 4) associated with O_2^- ions in the crystal TiO_2 structure, and when also Cu_2O is present additional peaks are present at 532.7 and 535.3 eV, corresponding to hydroxyl groups and water molecules adsorbed on the catalyst surface [65]. Moreover, the deconvolution of the spectra (Fig. 4B) allowed to clearly separate and distinguish the two peaks relating to adsorbed H_2O, O_2^- and OH^-. The presence of oxygen vacancies enhances the adsorption capacity of the catalysts' surface towards water and hydroxyl radicals, thus increasing the H^+ adsorption and H_2 formation [66,67].

The spectrum related to Cu 2p shows four peaks. The binding-energy component at approximately 937 eV, together with the shake-up satellite at around 946 eV (about 9 eV higher), is characteristic of Cu^{2+} [51]. The lower-energy peak at 934–935 eV is narrower and can be assigned to Cu^+, together the one at ca. 957.4 eV [51,68]. The broadness of the peaks suggests that some $Cu(OH)_2$ is also present. The detection of Cu_2O by XRD indicates that the bulk of the material is primarily composed of Cu_2O whilst the surface Cu^+ species were likely partially oxidized to Cu^{2+} during the XPS measurement, owing to the high instability and easy oxidizability of copper [51]. Notably, the intensity ratio of the copper peaks Cu $2p_{3/2}$ and Cu $2p_{1/2}$ does not correspond to the ideal value equal about 2:1 because the Cu 2p spectrum is sensitive to the chemical environment of the copper atom [69–71]. In our case, the co-existence of different oxidation states of Cu contributes to altering the intensity ratio.

In Fig. 5, the EPR spectra recorded under dark and irradiation for the 3 %Cu_2O-TiO_2 photocatalyst are reported. In the presence of DMPO and H_2O_2 (Fig. 5A), weak signals related to hydroxyl radicals can be detected both in the absence and the presence of light, underlining the possible formation of a certain amount of $^{\bullet}OH$ radicals. The appearance of hydroxyl radicals in the absence of light is due to the interaction between TiO_2 and H_2O_2, as reported by Lee et al. [72]. The same authors stated that under irradiation, superoxide anionic radicals can preferentially form in the presence of TiO_2 and H_2O_2. Thus, the low EPR signal intensity of Cu_2O-TiO_2 under light (relative to dark) with peroxide occurs because the photoexcited charges are trapped by H_2O_2, an efficient scavenger, preventing $^{\bullet}OH$ radicals from accumulating to detectable levels.

In the solution containing H_2O/DMPO/MeOH (Fig. 5B), no EPR signal is present in the absence of light, indicating that the photocatalyst did not generate superoxide anion radicals ($^{\bullet}O_2^-$) in the dark; under irradiation, instead, the characteristic peaks attributed to the paramagnetic resonance peaks of the DMPO-$^{\bullet}O_2^-$ adduct [73,74] are visible.

Photoelectrochemical measurements were performed to investigate the impact of Cu_2O addition on the electronic properties of TiO_2. The photocurrent spectra, recorded in 0.1 M ABE at the open-circuit potential (80 mV and 120 mV vs. Ag/AgCl for TiO_2 and 3 %Cu_2O-TiO_2, respectively), are presented in Figs. 6A and B. In particular, while for bare TiO_2 only one peak is present, for 3 %Cu_2O-TiO_2, two peaks are visible and a maximum of the photocurrent appears between 350 nm

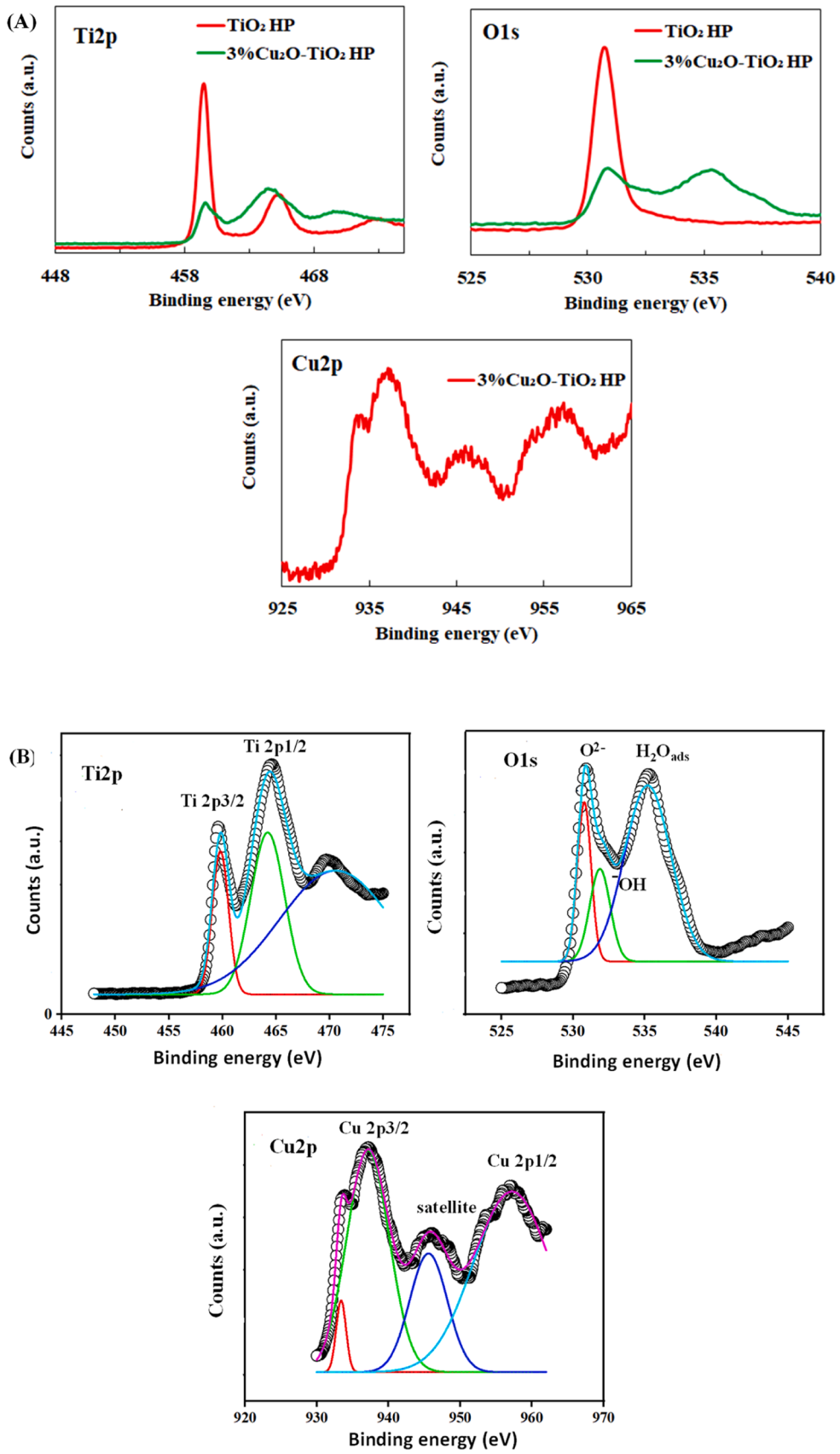

Fig. 4. XPS spectra related to Ti 2p, O 1 s, and Cu 2p regions (A) and their deconvolution (B) for TiO_2 and 3 %Cu_2O-TiO_2 samples.

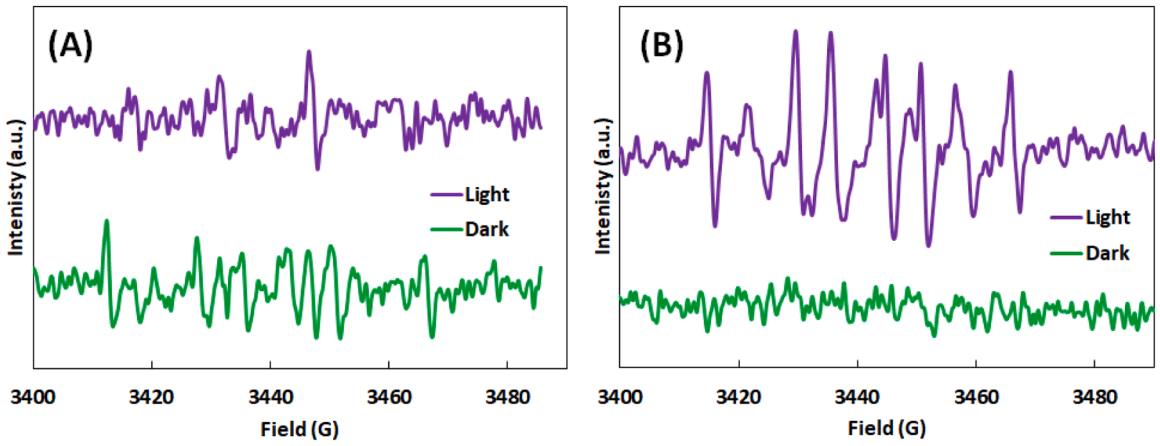

Fig. 5. EPR spectra of the 3 %Cu_2O-TiO_2 sample under dark and light irradiation: (A) sample dispersed in H_2O/DMPO/H_2O_2 solution, and (B) sample dispersed in H_2O/DMPO/MeOH solution.

and 400 nm, indicating the presence of electronic transitions between the two components. In the photocurrent spectra of 3 % Cu_2O-TiO_2 (Fig. 6B), slightly enhanced visible light absorption can be observed compared to pure TiO_2, in accordance with DRS spectra. However, given the low loading of Cu_2O relative to TiO_2 and the high recombination rate of charge carriers in Cu_2O (as evidenced by the absence of photocurrent in pure Cu_2O), it can be concluded that the overall photocurrent response is predominantly governed by TiO_2. This supports the UV absorption by TiO_2, followed by charge carrier separation by TiO_2-Cu_2O heterojunctions, rather than visible light absorption by Cu_2O.

Assuming non-direct optical transitions, the optical band gap values (E_g) of the studied photocatalysts can be determined using Equation (1):

$$(Q_{ph} \bullet h\nu)^{0.5} \propto (h\nu - E_g) \quad (1)$$

where $h\nu$ is the photon energy, and Q_{ph} represents the photocurrent yield, corrected for the efficiency of the lamp monochromator system. Since this correction is proportional to the light absorption coefficient near the band gap, the optical band gaps are estimated by extrapolating the $(Q_{ph} \bullet h\nu)^{0.5}$ vs. $h\nu$ plots to zero (Figs. 6C and D).

For TiO_2, an E_g of 3.2 eV was determined, whereas for 3 %Cu_2O-TiO_2, two band gaps were identified at 3.0 eV, related to TiO_2, and at 2.1 eV attributed to Cu_2O. The presence of photocurrent at photon energies below the TiO_2 band gap suggests optical transitions within Cu_2O, which has a lower band gap than TiO_2 polymorphs.

Fig. 6E and F illustrate the effect of light irradiation on the open-circuit potential (OCP) for TiO_2 and 3 %Cu_2O-TiO_2 under the same experimental conditions. Upon irradiation, OCP shifts negatively for TiO_2, consistent with n-type semiconductor performance. This behaviour is further confirmed by transient current measurements, where manual interrupting irradiation results in an anodic photocurrent (Fig. 6G). However, for 3 %Cu_2O-TiO_2, a less negative photopotential is observed due to the opposing effects of light irradiation on n-type TiO_2 (negative shift) and p-type Cu_2O (positive shift) (Fig. 6F). This is in accordance with transient photocurrent data (Fig. 6H) recorded for the 3 %Cu_2O-TiO_2 sample, which show an initial cathodic photocurrent spike followed by a steady anodic photocurrent. After irradiation, conduction band electrons from Cu_2O initially generate a cathodic photocurrent. However, the interfacial built-in potential directs electrons toward the current collector while holes migrate toward the oxide/electrolyte interface, ultimately generating an anodic photocurrent.

3.2. Photocatalytic activity results

To evaluate the effect of Cu_2O coupled with TiO_2 HP for H_2 formation, the photoreforming of different sacrificial agents was studied. In particular, formic acid, ethanol, glucose and glycerol were used. The group of sacrificial agents was selected due to their low splitting energy demand of 32.9, 29, 46.7 and 3.9 kJ·mol^{-1}, respectively, compared to 237.13 kJ·mol^{-1} for pure water. Furthermore, the appropriate position of their redox potential with respect to the valence band energy of the semiconductor makes them suitable for trapping photogenerated holes capable of oxidizing organic substances.

The 3 %Cu_2O-TiO_2 HP sample was initially chosen as the photocatalyst only to select the sacrificial agent with which to subsequently conduct the optimization of the amount of Cu_2O in TiO_2 HP, since previous work carried out in lab-scale reactors with commercial TiO_2 instead of TiO_2 HP indicated that the 3 % Cu_2O percentage gave the best results [18,75].

The use of sacrificial agents such as ethanol and glucose resulted in poor H_2 generation, yielding 4.1 mmol (STH of 0.13 %) and 3.4 mmol (STH of 0.11 %) respectively, at H_{UV} of 420 kJ·m^{-2}, as shown in Fig. 7. The highest H_2 amount was obtained adding glycerol and formic acid as sacrificial compounds. In particular, the amount of H_2 generated with formic acid (Fig. 7) was 33.9 mmol (STH of 1.05 %), very similar to that measured with glycerol (STH of 1.07 %) at 420 kJ·m^{-2}. The results obtained are in accordance with literature data. Chen et al. [76] investigated the activity of Au/TiO_2 photocatalysts in alcohols–H_2O mixtures and the H_2 production followed the order: glycerol > ethylene glycol > methanol > ethanol. Bowker [77], meanwhile, found that the rate decreased in the order glycerol > glucose > methanol > ethanol. Bahruji et al. [78], analyzing the behaviour of 20 different starting compounds, found the following reactivity order: triols > diols > 2 ° alcohols > 1 ° alcohols > 3 ° alcohols and assumed that the sacrificial agent displaying an α-H adjacent to the OH group(s) has a higher H_2 production activity.

Ethanol contains a single α-H adjacent to the hydroxyl group, which provides less reactive sites for oxidation reactions, and glucose, also displaying an α-H adjacent to the OH group, has a complex molecular structure and may require more energy to break down into H_2 and other intermediates before its mineralization. Formic acid has the simplest molecular structure that undergoes simple reactions producing H_2 and CO_2, and the single carboxyl group in its molecule facilitates a highly efficient pathway for electron donation to form H_2. Glycerol containing three hydroxyl groups is easy to oxidize, and provides more reactive sites, resulting in high H_2 generation. Features such as the presence of several hydroxyl groups in the structure, the length of the carbon chain, and dehydrogenation characteristics of sacrificial agents have a direct effect on H_2 generation [79]. Additionally, some other characteristics including polarity, the ability to be adsorbed by the surface of the photocatalyst and the production of byproducts, could have a significant impact on H_2 production efficiency and intermediate products [80,81]. The obtained results confirmed the effectiveness of Cu_2O in replacing

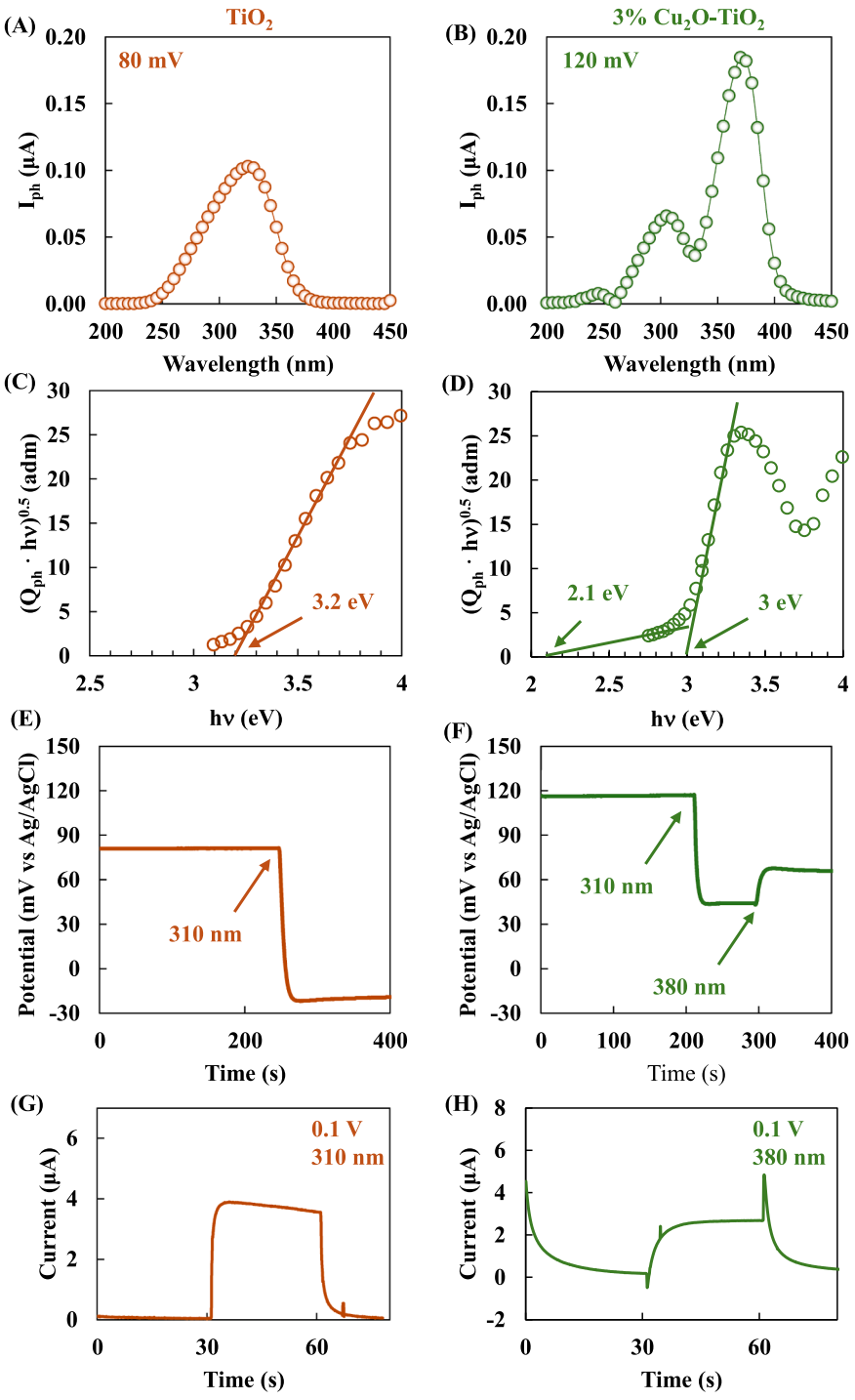

Fig. 6. Photocurrent spectra for A) TiO_2, B) 3 %Cu_2O-TiO_2, recorded in ABE 0.1 M solution. C) and D) show the respective $(Q_{ph} \cdot h\nu)^{0.5}$ vs hν plots. Photopotential, recorded in ABE 0.1 M for TiO_2 and 3 %Cu_2O-TiO_2, are reported in E) and F), respectively. G) and H) show the current–time transients recorded for TiO_2 and 3 % Cu_2O-TiO_2, respectively.

noble metals for H_2 production under solar irradiation and the formation of an efficient Cu_2O/TiO_2 heterostructure.

The highest amount of H_2 was produced in the presence of both formic acid and glycerol, but while formic acid is a valuable chemical in the pharmaceutical, chemical, agricultural and textile industries, glycerol is a waste product. For this reason the latter was used as a sacrificial agent to optimize the Cu_2O/TiO_2 HP ratio.

The used concentration of glycerol was 0.075 M, as determined in a previous study [82]. In Fig. 8, the amount of produced H_2 by using different Cu_2O TiO_2 HP photocatalysts is plotted versus H_{UV}. Results were compared at H_{UV} 660 ± 5 kJ·m^{-2} (value obtained after approximately 4.5 h of irradiation), since it was common to all tests. In the presence of 1 %Cu_2O-TiO_2 HP a H_2 evolution of 42.2 mmol (STH of 0.86 %) was obtained, suggesting the effectiveness of the Cu_2O-TiO_2 HP heterostructure [18]. The increase of Cu_2O into TiO_2 had a positive effect on H_2 formation, and with the 3 %Cu_2O-TiO_2 HP sample was 53.1 mmol (STH of 1.10 %), 26 % higher than that of 1 %Cu_2O-TiO_2 HP. However, by further increasing the amount of Cu_2O in TiO_2, the H_2 production efficiency decreased, being 48.3 mmol (STH of 0.99 %) the H_2 obtained in the presence of the 5 % Cu_2O-TiO_2 HP sample, as shown

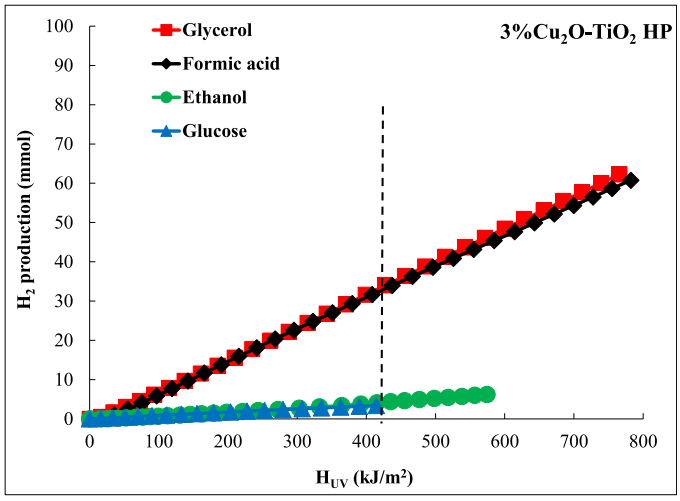

Fig. 7. H_2 generation with glycerol, formic acid, ethanol, and glucose in the presence of 3 %Cu_2O-TiO_2 HP.

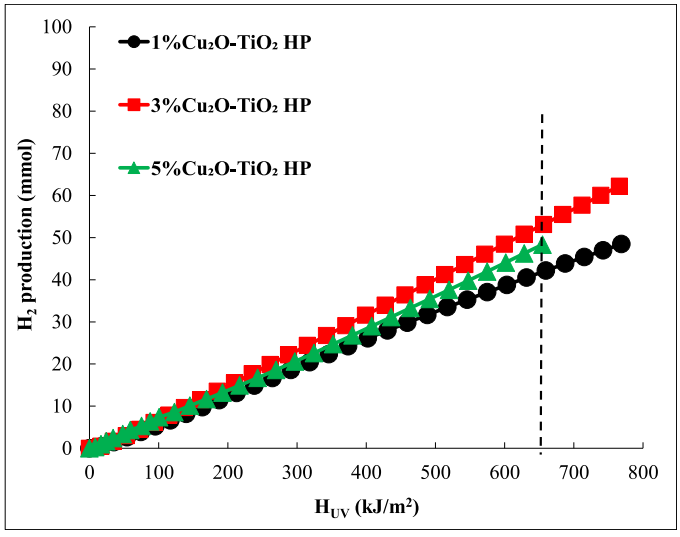

Fig. 8. H_2 generation with 1 %Cu_2O-TiO_2 HP, 3 %Cu_2O-TiO_2 HP, and 5 % Cu_2O-TiO_2 HP (Glycerol 0.075 M, 100 mg·L^{-1} photocatalyst).

in Fig. 8.

It can be stated that at the lowest percentage (1 %) there was a lower number of active sites due to the addition of Cu_2O to form the composite, compared to the sample with 3 %, while at the highest amount (5 %) a higher number of sites on the TiO_2 surface were covered and therefore deactivated since the light could not reach them. The amount of 3 % of Cu_2O has proven to be the best among those used favoring the formation of an optimal number of surface-active sites of TiO_2 and Cu_2O, also inducing a good mutual interaction between the two components [78], in accordance with photoluminescence results. An excessive increase of Cu_2O can produce the formation of agglomerates and reduce the effectiveness of the Cu_2O-TiO_2 HP heterojunction, essential for a high photocatalytic production of H_2. Furthermore, the decrease of the absorbed light, due to the TiO_2 covering effect, reduces the ability to generate electron-hole pairs. The low difference in the specific surface area values does not justify the different photoactivity of the various samples.

The formation of H_2 in the presence of Cu_2O-TiO_2 HP photocatalysts can be explained by assuming a charge transfer between the components (Fig. 9) [51]. When two different polymorphs of TiO_2 are present, the surface phase junction between them enables an effective electron transfer between the particles, which results in an efficient charge separation. Particularly, the CB edge of anatase being more negative than that of rutile, electrons, after irradiation, will transfer from the former to the second phase and, due to the slightly more positive value of the VB edge of anatase with respect to rutile, holes will be transferred from anatase to the VB of rutile [83]. However, it cannot be excluded the formation of a Type II heterojunction between anatase and rutile instead of Type I. In fact, while the energy values of the valence and conduction band edges of commercial TiO_2 samples prepared at high temperatures can be precisely determined, this cannot be done with samples prepared in the laboratory under mild experimental conditions. In these cases, the presence of amorphous matter [84] and defects, and the particle size [85], can slightly shift the bands' position [86]. Furthermore, when a p-Type semiconductor (as Cu_2O) is in contact with an n-type semiconductor (as TiO_2), an internal electric field will be formed at the interface, which will generate a movement of charges according to a Type-II heterojunction [45]. In addition, under solar light irradiation, photoexcited e^-/h^+ pairs are produced in both Cu_2O and TiO_2. Considering the energy band levels of rutile and Cu_2O, holes will transfer from the VB of TiO_2 to the VB of Cu_2O and electrons from the CB of Cu_2O to the CB of TiO_2. The holes accumulated in the VB of Cu_2O will oxidize sacrificial agents, producing organic intermediates, CO_2 and H^+ ions whilst the electrons collected in the rutile TiO_2 CB will reduce H^+ to H_2. These charge transfers significantly reduce the recombination of photogenerated charges as indicated by PL results, thus increasing the

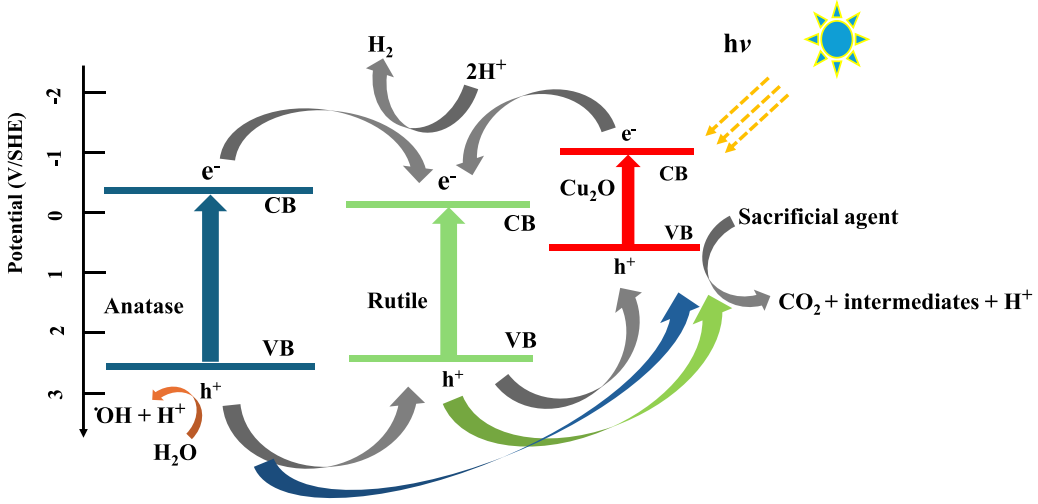

Fig. 9. Proposed reaction mechanism for H_2 generation in the presence of Cu_2O-TiO_2 HP.

photocatalytic capacity of the composites for H_2 production. Considering the VB energy of anatase and rutile, it is not excluded that glycerol oxidation occurs directly through the holes generated in these polymorphs. It should be noted that the H_2 produced during photoreforming comes not only from the dehydrogenation of the sacrificial agents but also from water [66,84] according to the following reaction:

$$ROH + H_2O \xrightarrow{Cu_2O/TiO_2, h\nu} H_2 + CO_2 + \text{value added compounds}$$

Some results confirm this: in pure water a very low quantity of H_2 was obtained; when organic sacrificial agents are present, the quantity of H_2 increased by increasing the quantity of the latter and was greater than that calculated stoichiometrically considering their conversion [87]. The positive effect of Cu_2O on H_2 production can be attributed both to the formation of an effective heterojunction and to the instability of Cu^+ ions (they could be oxidized to Cu^{2+} by holes), making electrons more available for the reduction of H^+ ions to H_2.

Notably, the color of CPC tubes under irradiation was turned into garnet-purple, this could be due to the formation of some amount of Ti^{3+} species (blue colored) attributed to the transfer of electrons from Cu^+ to Ti^{4+} with the formation of Cu^{2+} species and/or the formation of some amounts of Cu^0, in accordance with the literature [42]. Both species can play a positive role on photoactivity as Ti^{3+} creates electronic states below the conduction band responsible for visible light absorption, while Cu^0 takes part to redox processes, enhancing the charges transfer process [88,89].

This is also in accordance with the scheme reported in Fig. 9, which justifies the transfer of holes from TiO_2 to Cu_2O. The purple-garnet color of the reaction mixture, mentioned above, could actually be due to a mixture of blue (Ti^{3+}) and red (Cu_2O) and/or to the presence of Cu^0, although it is difficult to establish and is only a visual evidence, albeit useful. A study on the occurrence and extent of possible copper leaching is reported below in section 3.3.

During photoreforming, the formation of short-chain carboxylic acids (Fig. 10) was followed by ionic chromatography. Fig. 10A shows the evolution of formic acid (FA) during the photoreforming of glycerol. It was the main product, but probably other compounds formed in traces, such as glycolic acid (GA), were not detected as below the quantification limit of the analytical protocol. However, it can also be assumed that other reaction products were probably rapidly converted into formic acid. The partial oxidation of the initial substrate was faster than the mineralization of formic acid, and therefore this acid was able to accumulate in the water.

The highest formic acid amount was observed with 3 %Cu_2O-TiO_2 HP, which also gave the highest H_2 production. This result can be explained by considering that a greater use of holes for the glycerol oxidation reaction corresponds to a greater availability of electrons for the reduction of H^+, confirming the fundamental role of sacrificial agents for the production of H_2.

FA was also the main measured intermediate product (before mineralization) deriving from glucose (Fig. 10B); in the presence of ethanol, only small quantities of FA were observed, in agreement with the low production of H_2. Traces of GA and acetic acid were also detected but not reported for the sake of brevity.

During the experiments, except when formic acid was used as sacrificial agent, a decrease in pH from ~7.5 to ~4.5 was observed. When formic acid was used as sacrificial agent, since the decrease in pH with the other sacrificial agents was due to the formation of short-chain carboxylic acids, the pH remained almost unchanged at the initial value provided by formic acid (pH ~ 3.3). The temperature of the reaction system increased significantly during the tests, i.e. from ~29 °C to ~52 °C, but this did not cause any significant change in the rate of H_2 formation (Figs. 7 and 8), as is usual in heterogeneous photocatalysis and discussed in the literature [80].

In Fig. 11A the results obtained during the glycerol photoreforming in the absence and in the presence of scavengers as tert-butanol (for

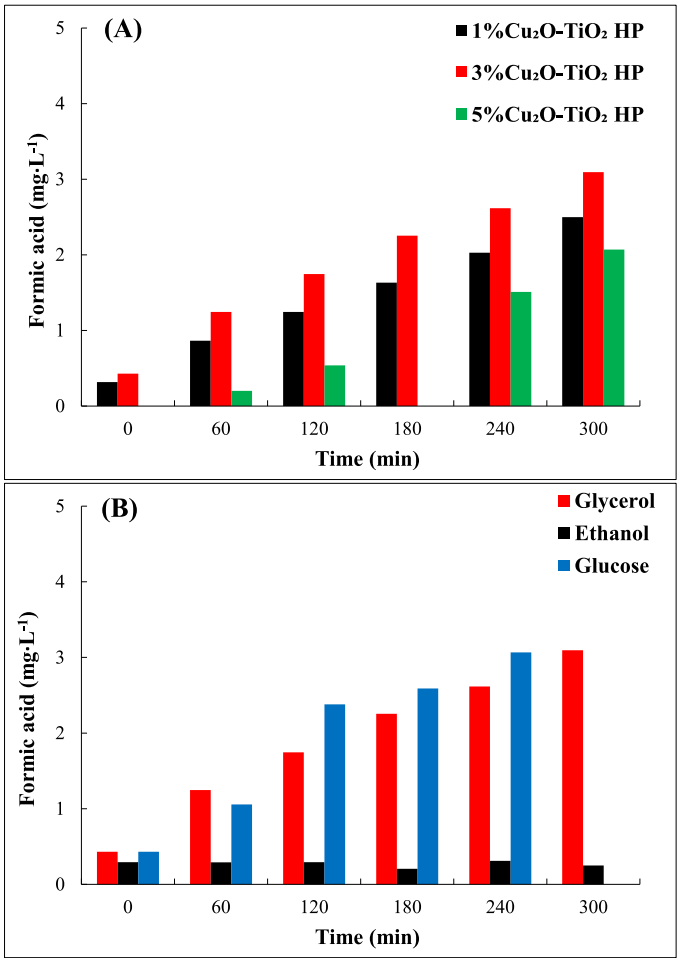

Fig. 10. (A) Formation of formic acid (FA) with different photocatalysts in the presence of glycerol as a sacrificial agent. (B) Formation of FA with glycerol, ethanol and glucose as sacrificial agents in the presence 3 %Cu_2O-TiO_2 HP.

hydroxyl radicals), $Na_2C_2O_4$ (for holes), $AgNO_3$ (for electrons) and benzoquinone (for superoxide ions) using 3 %Cu_2O-TiO_2 HP as photocatalyst under simulated solar light irradiation are reported. Notably, the formation of the superoxide radical can be attributed to the small amount of residual oxygen adsorbed onto the photocatalyst surface. These experiments were conducted solely to investigate the mechanistic aspects of the photoreaction and to identify the primary reactive species involved in glycerol degradation. Quantitative comparison with the tests performed in the pilot reactor is not feasible, as it is well established that numerical correlations cannot be drawn when the reaction setups differ fundamentally.

While in the presence of tert-butanol, sodium oxalate and benzoquinone a lower conversion of glycerol is observed, after the addition of silver nitrate an increase in photoactivity is measured. These results suggest that the removal from the reaction mixture of $OH^\bullet$ radicals, h^+ and $O_2^{\bullet-}$ radicals was detrimental as all species intervene in the glycerol oxidation process, but the holes and superoxide radicals play the predominant role, in accordance with EPR spectra.

On the contrary, in the presence of $AgNO_3$, an increase in conversion is observed, which highlights how the removal of electrons makes more holes available for the oxidation process. The respective amounts of H_2 and CO_2 obtained (Fig. 11B) confirm these results.

Namely, following the addition of tert-butanol and $Na_2C_2O_4$, the production of H_2 and CO_2 was lower than that obtained in the absence of scavengers. No H_2 was obtained, and a higher amount of CO_2 was formed when electrons and superoxide anions were removed. The

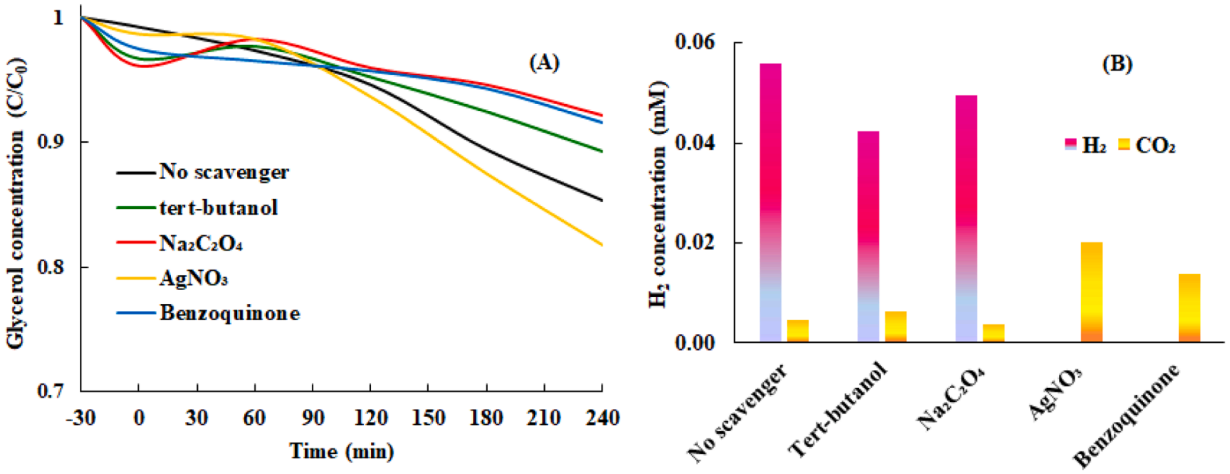

Fig. 11. Glycerol concentration versus irradiation time (A) and H_2 and CO_2 amount after 4 h of irradiation (B) by using 3 %Cu_2O-TiO_2 HP with and without scavenging species.

higher degree of mineralization, therefore, can be attributed to the higher availability of holes after the removal of e^- and $O_2^{\bullet-}$ by the scavengers, $AgNO_3$ and benzoquinone, respectively.

3.3. Cu leaching

It is important to study the possible leaching of metals from photocatalysts during the photocatalytic reaction. During photoreforming, the formation of organic acids (and subsequent progressive decrease in the pH) can favour the dissolution of Cu oxides causing photo-corrosion [90]. Cu leaching was studied by ICP-MS under the best experimental conditions, i.e, with 3 %Cu_2O-TiO_2 HP and glycerol. During the irradiation, the Cu content in the solution increased and the leaching before the irradiation and after 5 h of reaction was 0.32 and 2.16 mg·L^{-1}, respectively (notably, this value must be evaluated considering that 2.5 g of catalyst were used for each test). To further investigate this aspect, the elementary composition of the sample 3 %Cu_2O-TiO_2 HP was examined by an electron microprobe working in an energy dispersive mode (EDX) before and after the photocatalytic runs. The atomic Cu amount on the "fresh" 3 %Cu_2O-TiO_2 HP was 1.35 wt%, very close to the nominal one (1.20 wt%) while after the recovery at the end of the run, the amount drops to 0.93 % confirming the occurrence of a moderate copper leak, visually evidenced by the change in color of the reaction mixture during irradiation.

Cu leaching is a negative issue; however, this work can be considered as an initial study demonstrating the efficacy of a simple and eco-friendly ball milling method to prepare photocatalytic systems containing semiconductors more stable than Cu_2O for H_2 production on a pilot scale in noble metal free conditions. Various approaches, such doping, surface passivation and other modification methods, can be explored to fine-tune the surface properties of Cu_2O, improving its photocorrosion resistance and thus increasing its stability. However, it is reasonable to assume that the instability of Cu_2O is mitigated by the coupling with TiO_2 compared to the pure oxide. The intimate contact between Cu_2O and TiO_2 facilitates the rapid electrons transfer from Cu_2O to TiO_2, reducing recombination and photocorrosion.

A thorough and dedicated study of the various technologies is necessary to evaluate the pros and cons of the different approaches. Passivation, for example, consists in coating a material so that it becomes "passive", that is, less readily corroded by the environment. However, passivation involves the formation of an outer layer of shield material that can decrease the photoactivity by covering the active sites of the catalyst.

4. Conclusions

Coupling Cu_2O with home-prepared TiO_2 was successful for solar-to-hydrogen (STH) conversion in a pilot plant photoreactor. The TiO_2/Cu_2O composites showed an enhanced response under solar light irradiation and good activity for H_2 production [71]. The formation of p-n heterojunction, as confirmed by electrochemical and photoluminescence measurements, induces charges separation, the formation of oxygen vacancies and increased water adsorption capability which result in good photocatalytic activity. The produced H_2 followed the order: glycerol ≈ formic acid > ethanol ≈ glucose and 62 mmol were obtained after 5 h of natural sun-light irradiation (corresponding to an H_2 evolution rate of ca. 5 mmol g^{-1} h^{-1}) by using glycerol as sacrificial agent. Mechanistic investigation carried out in a lab-scale reactor by following the glycerol reforming in the presence of selected scavengers confirmed that h^+, $OH^\bullet$ and $O_2^{\bullet-}$ radicals are active species for glycerol degradation whilst electrons have the leading role in the reduction of H^+ ions to H_2. Although a moderate leaching of Cu species has been observed after the photocatalytic runs, however the facile preparation of composite photocatalysts, active for solar H_2 production without the use of noble metals, deserves to be further explored. Metal leaching from photocatalysts is rarely examined in literature, yet it represents a critical aspect of evaluating any newly proposed material for these applications. In this study, we place particular emphasis on assessing this issue. Future studies, moreover, should be addressed to increase the stability of the photocatalyst to eliminate or significantly reduce leaching.

CRediT authorship contribution statement

Leonardo Palmisano: Writing – review & editing. **Ilaria Berruti:** Writing – review & editing, Supervision. **Vittorio Loddo:** Writing – review & editing. **Sixto Malato Rodríguez:** Writing – review & editing, Supervision, Funding acquisition. **Marianna Bellardita:** Writing – review & editing, Supervision, Data curation, Conceptualization. **Alba Ruiz-Aguirre:** Writing – review & editing, Supervision. **Muhammad Umair:** Writing – original draft, Investigation.

Declaration of Competing Interest

The authors declare that they have no known competing financial interests or personal relationships that could have appeared to influence the work reported in this paper.

Acknowledgments

CIEMAT – Plataforma Solar de Almería wish to thank the Grant PID2024-159086OB-C33 (PHOTOREDVALORA) funded by MICIU/AEI/10.13039/501100011033 and by FSE+ for partial financing of this study. The Authors thank Prof. Giovanni Palmisano (Khalifa University, Abu Dhabi, UAE) for TEM, XPS and EPR measurements, Dr. Anna Maria Venezia (ISMN-CNR) for XPS discussion and Dr. Caludio Maria Pecoraro (University of Palermo) for electrochemical characterizations.

Appendix A. Supporting information

Supplementary data associated with this article can be found in the online version at doi:10.1016/j.cattod.2026.115740

Data Availability

No data was used for the research described in the article.

References

[1] P.J. Megía, A.J. Vizcaíno, J.A. Calles, A. Carrero, Hydrogen production technologies: from fossil fuels toward renewable sources. A mini review, Energy Fuels 35 (20) (2014) 16403–16415, https://doi.org/10.1021/acs.energyfuels.1c02501.

[2] F. Dawood, M. Anda, G.M. Shafiullah, Hydrogen production for energy: an overview, Int. J. Hydrog. Energy 45 (7) (2020) 3847–3869, https://doi.org/10.1016/j.ijhydene.2019.12.059.

[3] T. Ishaq, M. Yousaf, I.A. Bhatti, A. Batool, M.A. Asghar, M. Mohsin, M. Ahmad, A perspective on possible amendments in semiconductors for enhanced photocatalytic hydrogen generation by water splitting, Int. J. Hydrog. Energy 46 (79) (2021) 39036–39057, https://doi.org/10.1016/j.ijhydene.2021.09.165.

[4] European Commission, in: Communication from the Commission to the European Parliament, the European Council, the Council, the European Economic and Social Committee and the Committee of the Regions: The European Green Deal, European Commission, Brussels, 2019. https://eur-lex.europa.eu/legal-content/EN/TXT/?uri=CELEX%3A52019DC0640.

[5] D. Lei, L. Wang, Y. Lv, N. Luo, Z. Wang, Engineering applications of solar photocatalysis and photothermal catalysis for hydrogen production from biomass: a review, Chem. Eur. J. (2024) e202401486, https://doi.org/10.1002/chem.202401486.

[6] P. Afanasev, A. Askarova, T. Alekhina, E. Popov, S. Markovic, A. Mukhametdinova, A. Cheremisin, E. Mukhina, An overview of hydrogen production methods: focus on hydrocarbon feedstock, Int. J. Hydrog. Energy 78 (2024) 805–828, https://doi.org/10.1016/j.ijhydene.2024.06.369.

[7] G. Xie, K. Zhang, B. Guo, Q. Liu, L. Fang, J.R. Gong, Graphene-based materials for hydrogen generation from light-driven water splitting, Adv. Mater. 25 (28) (2013) 3820–3839, https://doi.org/10.1002/adma.201301207.

[8] T. Montini, M. Monai, A. Beltram, I. Romero-Ocaña, P. Fornasiero, H_2 production by photocatalytic reforming of oxygenated compounds using TiO_2-based materials, Mater. Sci. Semicond. Process. 42 (1) (2016) 122–130, https://doi.org/10.1016/j.mssp.2015.06.069.

[9] S. Rajendran, S. Saju, T. Mathew, C.S. Gopinath, Concurrent utilization of e^- and h^+ for water splitting to H_2 and biomass components into value-added products: sustainable solar-driven photocatalysis towards meeting SDG7, 12 and 13, Chem. Commun. 61 (86) (2025) 16738–16769, https://doi.org/10.1039/D5CC04056F.

[10] K. Shimura, H. Yoshida, Heterogeneous photocatalytic hydrogen production from water and biomass derivatives, Energy Environ. Sci. 4 (7) (2011) 2467–2481, https://doi.org/10.1039/c1ee01120k.

[11] W. Rulkens, Sewage sludge as a biomass resource for the production of energy: Overview and assessment of the various options, Energy Fuels 22 (1) (2008) 9–15, https://doi.org/10.1021/ef700267m.

[12] P. Liu, Z. Cai, Y. You, H. Huang, S. Chen, C. Gao, Z. Qi, et al., Surface modification on Pd–TiO_2 hybrid nanostructures towards highly efficient H_2 production from catalytic formic acid decomposition, Chem. Eur. J. 24 (69) (2018) 18398–18402, https://doi.org/10.1002/chem.201803267.

[13] Z. Zhang, S.-W. Cao, Y. Liao, C. Xue, Selective photocatalytic decomposition of formic acid over AuPd nanoparticle-decorated TiO_2 nanofibers toward high-yield hydrogen production, Appl. Catal. B Environ. 162 (2015) 204–209, https://doi.org/10.1016/j.apcatb.2014.06.055.

[14] M. Umair, G. Palmisano, R. Al Sakkaf, S. Al Jitan, A. Pintar, G. Žerjav, et al., Pt–Nb_2O_5–TiO_2 based semiconductors for photo-reforming of glucose and fructose aqueous solutions, Appl. Surf. Sci. 648 (2024) 159030, https://doi.org/10.1016/j.apsusc.2023.159030.

[15] L. Da Vià, C. Recchi, E.O. Gonzalez-Yañez, T.E. Davies, J.A. Lopez-Sanchez, Visible light selective photocatalytic conversion of glucose by TiO_2, Appl. Catal. B Environ. 202 (2017) 281–288, https://doi.org/10.1016/j.apcatb.2016.08.035.

[16] X. Luo, X. Ge, S. Cui, Y. Li, Value-added processing of crude glycerol into chemicals and polymers, Bioresour. Technol. 215 (2016) 144–154, https://doi.org/10.1016/j.biortech.2016.03.042.

[17] C.R. Coronado, J.A. Carvalho, C.A. Quispe, C.R. Sotomonte, Ecological efficiency in glycerol combustion, Appl. Therm. Eng. 63 (2014) 97–104, https://doi.org/10.1016/j.applthermaleng.2013.11.004.

[18] C.M. Pecoraro, M. Bellardita, V. Loddo, F. Di Franco, L. Palmisano, M. Santamaria, A facile way to synthesize noble metal free TiO_2-based catalysts for glycerol photoreforming, J. Ind. Eng. Chem. 118 (2023) 247–258, https://doi.org/10.1016/j.jiec.2022.11.010.

[19] V. Maurino, A. Bedini, M. Minella, F. Rubertelli, E. Pelizzetti, C. Minero, Glycerol transformation through photocatalysis: a possible route to value-added chemicals, J. Adv. Oxid. Technol. 11 (2008) 184–192, https://doi.org/10.1515/jaots-2008-0201.

[20] A. Fujishima, T.N. Rao, D.A. Tryk, Titanium dioxide photocatalysis, J. Photochem. 577 Photobiol. C 1 (2000) 1–21, https://doi.org/10.1016/S1389-5567(00)00002-2.

[21] J.A. Rengifo-Herrera, C. Pulgarin, Why five decades of massive research on heterogeneous photocatalysis, especially on TiO_2, has not yet driven to water disinfection and detoxification applications? Critical review of drawbacks and challenges, Chem. Eng. J. 477 (2023) 146875, https://doi.org/10.1016/j.cej.2023.146875.

[22] Y. Cai, Y.P. Feng, Review on charge transfer and chemical activity of TiO_2: mechanism and applications, Prog. Surf. Sci. 91 (2016) 183–202, https://doi.org/10.1016/j.progsurf.2016.11.001.

[23] M. Humayun, F. Raziq, A. Khan, W. Luo, Modification strategies of TiO_2 for potential applications in photocatalysis: a critical review, Green. Chem. Lett. Rev. 11 (2018) 86–102, https://doi.org/10.1080/17518253.2018.1440324.

[24] J. Chen, F. Qiu, W. Xu, S. Cao, H. Zhu, Recent progress in enhancing photocatalytic efficiency of TiO_2-based materials, Appl. Catal. A Gen. 495 (2015) 131–140, https://doi.org/10.1016/j.apcata.2015.02.013.

[25] A.R. Aguirre, A.C. Reina, J.P. Pérez, G. Colon, S. Malato, Catalysts and photoreactors for photocatalytic solar hydrogen production: fundamentals and recent developments at pilot scale, in: Photocatalytic Hydrogen Production for Sustainable Energy, Wiley, 2023, pp. 275–303, https://doi.org/10.1002/9783527835423.ch12.

[26] V. Kumaravel, S. Mathew, J. Bartlett, S.C. Pillai, Photocatalytic hydrogen production using metal-doped TiO_2: a review of recent advances, Appl. Catal. B Environ. 244 (2019) 1021–1064, https://doi.org/10.1016/j.apcatb.2018.11.080.

[27] M. Bellardita, E.I. García-López, G. Marcì, L. Palmisano, Photocatalytic formation of H_2 and value-added chemicals in aqueous glucose (Pt)-TiO_2 suspension, Int. J. Hydrog. Energy 41 (2016) 5934–5947, https://doi.org/10.1016/j.ijhydene.2016.02.103.

[28] J. Low, J. Yu, M. Jaroniec, S. Wageh, A.A. Al-Ghamdi, Heterojunction photocatalysts, Adv. Mater. 29 (2017) 1601694, https://doi.org/10.1002/adma.201601694.

[29] S. Meng, W. Sun, S. Zhang, X. Zheng, X. Fu, S. Chen, Insight into the transfer mechanism of photogenerated carriers for WO_3/TiO_2 heterojunction photocatalysts: Is it the transfer of band–band or Z-scheme? Why? J. Phys. Chem. C. 122 (2018) 26326–26336, https://doi.org/10.1021/acs.jpcc.8b07524.

[30] S. Zhang, Z. Liu, W. Yan, Z. Guo, M. Ruan, Decorating non-noble metal plasmonic Al on a TiO_2/Cu_2O photoanode to boost performance in photoelectrochemical water splitting, Chin. J. Catal. 41 (12) (2020) 1884–1893, https://doi.org/10.1016/S1872-2067(20)63637-3.

[31] X. Chen, M. Ruan, C. Wang, T. Zhong, Z. Liu, Phase engineering to construct In_2S_3 heterophase junctions and abundant active boundaries and surfaces for efficient pyro-PEC performance in CdS/In_2S_3, J. Mater. Chem. A 12 (25) (2024) 15440–15452, https://doi.org/10.1039/D4TA01455C.

[32] S. Zhang, Z. Liu, D. Chen, Z. Guo, M. Ruan, Oxygen vacancies engineering in TiO_2 homojunction/ZnFe-LDH for enhanced photoelectrochemical water oxidation, Chem. Eng. J. 395 (2020) 125101, https://doi.org/10.1016/j.cej.2020.125101.

[33] J. Feng, M. Cui, H. Liu, F. Zhou, S. Bi, D. Zhang, Design of an efficient photocatalyst: a type II heterojunction for enhanced hydrogen production driven by visible light, Phys. Chem. Chem. Phys. 23 (2021) 11893–11899, https://doi.org/10.1039/D1CP00347J.

[34] Y.-H. Zhang, M.-M. Liu, J.-L. Chen, K.-F. Xie, S.-M. Fang, Dendritic branching Z-scheme Cu_2O/TiO_2 heterostructure photocatalysts for boosting H_2 production, J. Phys. Chem. Solids 152 (2021) 109948, https://doi.org/10.1016/j.jpcs.2021.109948.

[35] M. Rafique, S. Hajra, M. Irshad, M. Usman, M. Imran, M.A. Assiri, et al., Hydrogen production using TiO_2-based photocatalysts: a comprehensive review, ACS Omega 8 (2023) 25640–25648, https://doi.org/10.1021/acsomega.3c00963.

[36] A. Di Paola, M. Bellardita, R. Ceccato, L. Palmisano, F. Parrino, Highly active photocatalytic TiO_2 powders obtained by thermohydrolysis of TiCl4 in water, J. Phys. Chem. C 113 (2009) 15166–15174, https://doi.org/10.1021/jp904673e.

[37] T. Ohno, K. Sarukawa, M. Matsumura, Photocatalytic activities of pure rutile particles isolated from TiO_2 powder by dissolving the anatase component in HF solution, J. Phys. Chem. B 105 (2001) 2417–2420, https://doi.org/10.1021/jp003211z.

[38] R.I. Bickley, T. Gonzalez-Carreno, J.S. Lees, L. Palmisano, R.J. Tilley, A structural investigation of titanium dioxide photocatalysts, J. Solid State Chem. 92 (1991) 178–190, https://doi.org/10.1016/0022-4596(91)90255-G.

[39] X. Jiang, M. Manawan, T. Feng, R. Qian, T. Zhao, G. Zhou, et al., Anatase and rutile in Evonik Aeroxide P25: heterojunctioned or individual nanoparticles? Catal. Today 300 (2018) 12–17, https://doi.org/10.1016/j.cattod.2017.06.010.

[40] D.C. Hurum, A.G. Agrios, K.A. Gray, T. Rajh, M.C. Thurnauer, Explaining the enhanced photocatalytic activity of Degussa P25 mixed-phase TiO_2 using EPR, J. Phys. Chem. B 107 (2003) 4545–4549, https://doi.org/10.1021/jp0273934.

[41] F. Parrino, M. Bellardita, E.I. García-López, G. Marcì, V. Loddo, L. Palmisano, Heterogeneous photocatalysis for selective formation of high-value-added molecules: Some chemical and engineering aspects, ACS Catal. 8 (2018) 11191–11225, https://doi.org/10.1021/acscatal.8b03093.
[42] F. Plascencia-Hernández, E. Albiter, G.M. Nawfal, C. Colbeau-Justin, H. Remita, H. Pfeiffer, M.A. Valenzuela, Unraveling the effect of low Cu_2O loading on P25 TiO_2 and its self-reduction during methanol photoreforming, Inorg. Chem. Commun. 158 (2023) 111541, https://doi.org/10.1016/j.inoche.2023.111541.
[43] E. do Couto-Pessanha, V.M. Paiva, M.D.R. Henriques, A.C. Rodrigues, F.E. Almeida, A. Berger, L.H. da Silva, M.J. Izumi, H.V. Fajardo, TiO_2/Cu_2O heterojunction with ultrafine Cu_2O dispersion and enhanced performance for solar-driven hydrogen production: a low-temperature, ambient pressure, and common stabilizing agent-free synthesis approach, ACS Omega 10 (2025) 39814–39822, https://doi.org/10.1021/acsomega.5c03805.
[44] S. Rajendran, S.S. Mani, T.R. Nivedhitha, A.K. Asoka, P.S. Arun, T. Mathew, C. S. Gopinath, Facile one-pot synthesis of CuxO/TiO_2 photocatalysts by regulating Cu oxidation state for efficient solar H_2 production, ACS Appl. Energy Mater. 7 (2023) 104–116, https://doi.org/10.1021/acsaem.3c02272.
[45] M.O. Segovia-Guzmán, M. Román-Aguirre, J.Y. Verde-Gomez, V.H. Collins-Martínez, G. Zaragoza-Galán, V.H. Ramos-Sánchez, Green Cu_2O/TiO_2 heterojunction for glycerol photoreforming, Catal. Today 349 (2020) 88–97, https://doi.org/10.1016/j.cattod.2018.05.031.
[46] J.-L. Chen, S.-Y. Xie, L.-J. Yue, F.-L. Gong, Y.-H. Zhang, Facile synthesis of Cu_2O/TiO_2 (P25) composites with enhanced photocatalytic H_2 evolution activity, J. Mater. Sci. Mater. Electron. 32 (2021) 18900–18911, https://doi.org/10.1007/s10854-021-06407-2.
[47] A.M. Djaballah, M. Bellardita, L. Palmisano, V. Loddo, M. Umair, C.M. Pecoraro, et al., Facile preparation of $CuBi_2O_4$/TiO_2 hetero-systems employed for simulated solar-light selective oxidation of 4-methoxybenzyl alcohol model compound, Mol. Catal. 546 (2023) 113251, https://doi.org/10.1016/j.mcat.2023.113251.
[48] A. Nigussie, H.C.A. Murthy, A. Bedassa, A review on synthesis, characterization and photocatalytic applications of copper oxide nanostructures, Res. J. Chem. Environ. 25 (2021) 6.
[49] J.G. Villachica-Llamosas, A. Ruiz-Aguirre, G. Colón, J. Peral, S. Malato, CuO–TiO_2 pilot-plant system performance for solar photocatalytic hydrogen production, Int. J. Hydrog. Energy 51 (2024) 1069–1077, https://doi.org/10.1016/j.ijhydene.2023.07.149.
[50] Q. Zhu, Y. Peng, L. Lin, C.-M. Fan, G.Q. Gao, R.-X. Wang, A.-W. Xu, Stable blue TiO_2−x nanoparticles for efficient visible light photocatalysts, J. Mater. Chem. A 2 (2014) 4429–4437, https://doi.org/10.1039/C3TA14484D.
[51] J.L. Chen, M.-M. Liu, S.-Y. Xie, L.-J. Yue, F.-L. Gong, K.-M. Chai, Y.-H. Zhang, Cu_2O-loaded TiO_2 heterojunction composites for enhanced photocatalytic H_2 production, J. Mol. Struct. 1247 (2022) 131294, https://doi.org/10.1016/j.molstruc.2021.131294.
[52] S. Obregón Alfaro, G. Colón Ibáñez, A ternary Er3+-BiVO4/TiO_2 complex heterostructure with excellent photocatalytic performance, RSC Adv. 4 (2014) 6920–6926, https://doi.org/10.1039/C3RA46603E.
[53] N.D. Abazović, M.I. Čomor, M.D. Dramićanin, D.J. Jovanović, S.P. Ahrenkiel, J. M. Nedeljković, Photoluminescence of anatase and rutile TiO_2 particles, J. Phys. Chem. B. 110 (2006) 25366–25370, https://doi.org/10.1021/jp064454f.
[54] D. Zhang, Synergetic effects of Cu_2O photocatalyst with titania and enhanced photoactivity under visible irradiation, Acta Chim. Slov. 6 (2013) 141–149, https://doi.org/10.2478/acs-2013-0022.
[55] M. Kouti, L. Matouri, Fabrication of nanosized cuprous oxide using Fehling's solution, Sci. Iran. 17 (2010) 73–78. https://api.semanticscholar.org/CorpusID:54534478 (Available from:).
[56] H.Z. Zhang, J.F. Banfield, Understanding polymorphic phase transformation behavior during growth of nanocrystalline aggregates: Insights from TiO_2, J. Phys. Chem. B 104 (2000) 3481–3487, https://doi.org/10.1021/jp000499j.
[57] R. Fiorenza, M. Bellardita, L. D'Urso, G. Compagnini, L. Palmisano, S. Scirè, Au/TiO_2-CeO2 catalysts for photocatalytic water splitting and VOCs oxidation reactions, Catalysts 6 (2016) 121, https://doi.org/10.3390/catal6080121.
[58] G. Liu, X. Yan, Z. Chen, X. Wang, L. Wang, G.Q. Lu, H.M. Cheng, Synthesis of rutile–anatase core–shell structured TiO_2 for photocatalysis, J. Mater. Chem. 19 (2009) 6590–6596, https://doi.org/10.1039/B902666E.
[59] L. Miao, P. Jin, K. Kaneko, A. Terai, N. Nabatova-Gabain, S. Tanemura, Preparation and characterization of polycrystalline anatase and rutile TiO_2 thin films by rf magnetron sputtering, Appl. Surf. Sci. 212–213 (2003) 255–263, https://doi.org/10.1016/S0169-4332(03)00106-5, 255263.
[60] D. Zhao, C.M. Tu, X.J. Hu, N. Zhang, Notable in situ surface transformation of Cu_2O nanomaterials leads to dramatic activity enhancement for CO oxidation, RSC Adv. 7 (2017) 37596–37603, https://doi.org/10.1039/C7RA05950G.
[61] A.K.R. Police, S.V.P. Vattikuti, K.K. Mandari, M. Chennaiahgari, Sharma M.v, D. K. Valluri, C. Byon, Bismuth oxide cocatalyst and copper oxide sensitizer in Cu_2O/TiO_2/Bi_2O_3 ternary photocatalyst for efficient hydrogen production under solar light irradiation, Ceram. Int. 44 (2018) 11783–11791, https://doi.org/10.1016/j.ceramint.2018.03.262.
[62] K.R. Park, D.T. Tran, T.T. Nguyen, N.H. Kim, J.H. Lee, Copper-incorporated heterostructures of amorphous NiSex/crystalline NiSe2 as an efficient electrocatalyst for overall water splitting, Chem. Eng. J. 422 (2021) 130048, https://doi.org/10.1016/j.cej.2021.130048.
[63] T. Wei, Y.N. Zhu, X.Q. An, L.M. Liu, X.Z. Cao, H.J. Liu, J.H. Qu, Defect modulation of Z-scheme TiO_2/Cu_2O photocatalysts for durable water splitting, ACS Catal. 9 (2019) 8346–8354, https://doi.org/10.1021/acscatal.9b01786.
[64] X. An, T. Li, B. Wen, J. Tang, Z. Hu, L.M. Liu, J. Qu, C.P. Huang, H. Liu, New insights into defect-mediated heterostructures for photoelectrochemical water splitting, Adv. Energy Mater. 6 (2016) 1502268, https://doi.org/10.1002/aenm.201502268.
[65] A. Wiatrowski, M. Mazur, A. Obstarczyk, D. Wojcieszak, D. Kaczmarek, J. Morgiel, D. Gibson, Comparison of the physicochemical properties of TiO_2 thin films obtained by magnetron sputtering with continuous and pulsed gas flow, Coatings 8 (2018) 412, https://doi.org/10.3390/coatings8110412.
[66] C.M. Pecoraro, L. Mino, E. Kozyr, L. Palmisano, F. di Franco, V. Loddo, M. Santamaria, M. Bellardita, Pt–TiO_2 catalysts for glycerol photoreforming: comparison of anatase, brookite and rutile polymorphs, Chem. Commun. 60 (2024) 3782–3785, https://doi.org/10.1039/D4CC00353E.
[67] H. Qian, B. Yuan, Y. Liu, R. Zhu, W. Luan, C. Zhang, Oxygen vacancy enhanced photocatalytic activity of Cu_2O/TiO_2 heterojunction, iScience 27 (2024) 109578, https://doi.org/10.1016/j.isci.2024.109578.
[68] K. Roy, C.S. Gopinath, UV photoelectron spectroscopy at near ambient pressures: mapping valence band electronic structure changes from Cu to CuO, Anal. Chem. 86 (8) (2014) 3683–3687, https://doi.org/10.1021/ac4041026.
[69] D. Cosma, A. Urda, T. Radu, M.C. Rosu, M. Mihet, C. Socaci, Evaluation of the photocatalytic properties of copper oxides/graphene/TiO_2 nanoparticles composites, Molecules 27 (2022) 5803, https://doi.org/10.3390/molecules27185803.
[70] P. Wang, Z. Liu, C. Han, et al., Cu_2O/CuO heterojunction formed by thermal oxidation and decorated with Pt co-catalyst as an efficient photocathode for photoelectrochemical water splitting, J. Nanopart. Res. 23 (2021) 268, https://doi.org/10.1007/s11051-021-05383-2.
[71] F.A. Akgul, G. Akgul, N. Yildirim, H.E. Unalan, R. Turan, Influence of thermal annealing on microstructural, morphological, optical properties and surface electronic structure of copper oxide thin films, Mater. Chem. Phys. 147 (2014) 987–995, https://doi.org/10.1016/j.matchemphys.2014.06.047.
[72] M.-C. Lee, F. Yoshino, H. Shoji, et al., Characterization by electron spin resonance spectroscopy of reactive oxygen species generated by titanium dioxide and hydrogen peroxide, J. Dent. Res. 84 (2) (2005) 178–182, https://doi.org/10.1177/154405910508400213.
[73] W. He, Y. Liu, W.G. Wamer, J.-J. Yin, Electron spin resonance spectroscopy for the study of nanomaterial-mediated generation of reactive oxygen species, J. Food Drug Anal. 22 (2014) 49–63, https://doi.org/10.1016/j.jfda.2014.01.004.
[74] J. Qiu, L. Zhang, D. Dai, G. Xia, J. Yao, Cellulose-derived carbon dot-guided growth of ZnIn2S4 nanosheets for photocatalytic oxidation of 5-hydroxymethylfurfural into 2,5-diformylfuran, ChemSusChem 15 (2022) e202200399, https://doi.org/10.1002/cssc.202200399.
[75] M. Muscetta, S.Al Jitan, G. Palmisano, R. Andreozzi, R. Marotta, S. Cimino, I. Di Somma, Visible light–driven photocatalytic hydrogen production using Cu_2O/TiO_2 composites prepared by facile mechanochemical synthesis, J. Environ. Chem. Eng. 10 (2022) 107735, https://doi.org/10.1016/j.jece.2022.107735.
[76] W.T. Chen, A. Chan, Z.H.N. Al-Azri, A.G. Dosado, M.A. Nadeem, D. Sun-Waterhouse, H. Idriss, G.I.N. Waterhouse, Effect of TiO_2 polymorph and alcohol sacrificial agent on the activity of Au/TiO_2 photocatalysts for H_2 production in alcohol–water mixtures, J. Catal. 329 (2015) 499–513, https://doi.org/10.1016/j.jcat.2015.06.014.
[77] M. Bowker, Photocatalytic hydrogen production and oxygenate photoreforming, Catal. Lett. 142 (2012) 923–929, https://doi.org/10.1007/s10562-012-0875-4.
[78] H. Bahruji, M. Bowker, P.R. Davies, F. Pedrono, New insights into the mechanism of photocatalytic reforming on Pd/TiO_2, Appl. Catal. B 107 (2011) 205–209, https://doi.org/10.1016/j.apcatb.2011.07.015.
[79] V. Kumaravel, M.D. Imam, A. Badreldin, R.K. Chava, J.Y. Do, M. Kang, A. Abdel-Wahab, Photocatalytic hydrogen production: Role of sacrificial reagents on the activity of oxide, carbon, and sulfide catalysts, Catalysts 9 (2019) 276, https://doi.org/10.3390/catal9030276.
[80] F.J. López-Tenllado, J. Hidalgo-Carrillo, V. Montes, A. Marinas, F.J. Urbano, J. M. Marinas, L. Ilieva, T. Tabakova, F. Reid, A comparative study of hydrogen photocatalytic production from glycerol and propan-2-ol on M/TiO_2 systems (M = Au, Pt, Pd), Catal. Today 280 (2017) 58–64, https://doi.org/10.1016/j.cattod.2016.05.009.
[81] O. Quiroz-Cardoso, S. Oros-Ruiz, A. Solís-Gómez, R. López, R. Gómez, Enhanced photocatalytic hydrogen production by CdS nanofibers modified with graphene oxide and nickel nanoparticles under visible light, Fuel 237 (2019) 227–235, https://doi.org/10.1016/j.fuel.2018.10.013.
[82] A. Ruiz-Aguirre, J.G. Villachica-Llamosas, M.I. Polo-López, A. Cabrera-Reina, G. Colón, J. Peral, S. Malato, Assessment of pilot-plant scale solar photocatalytic hydrogen generation with multiple approaches: valorization, water decontamination and disinfection, Energy 260 (2022) 125199, https://doi.org/10.1016/j.energy.2022.125199.
[83] D.C. Hurum, A.G. Agrios, K.A. Gray, T. Rajh, M.C. Thurnauer, Explaining the enhanced photocatalytic activity of Degussa P25 mixed-phase TiO_2 using EPR, J. Phys. Chem. B 107 (2003) 4545–4549, https://doi.org/10.1021/jp0273934.
[84] R.I. Bickley, T. Gonzalez-Carreno, J.S. Lees, L. Palmisano, R.J.D. Tilley, A structural investigation of titanium dioxide photocatalysts, J. Solid State Chem. 92 (1991) 178–190, https://doi.org/10.1016/0022-4596(91)90255-G.
[85] F.T. Rabouw, C. de Mello Donega, Excited-state dynamics in colloidal semiconductor nanocrystals, Top. Curr. Chem. 374 (2016) 58, https://doi.org/10.1007/s41061-016-0060-0.
[86] H. Zhao, F. Pan, Y. Li, A review on the effects of TiO_2 surface point defects on CO_2 photoreduction with H_2O, J. Mater. 3 (2017) 17–32, https://doi.org/10.1016/j.jmat.2016.12.001.
[87] G. Iervolino, V. Vaiano, J.J. Murcia, A.E. Lara, J.S. Hernández, H. Rojas, J. A. Navío, M.C. Hidalgo, Photocatalytic production of hydrogen and methane from

glycerol reforming over Pt/TiO_2–Nb_2O_5, Int. J. Hydrog. Energy 46 (78) (2021) 38678–38691, https://doi.org/10.1016/j.ijhydene.2021.09.111.
[88] N. Serpone, Is the band gap of pristine TiO_2 narrowed by anion- and cation-doping of titanium dioxide in second-generation photocatalysts? J. Phys. Chem. B 110 (2006) 24287–24293, https://doi.org/10.1021/jp065659r.
[89] Q. Zhu, Y. Peng, L. Lin, C.-M. Fan, G.-Q. Gao, R.-X. Wang, A.-W. Xu, Stable blue TiO_{2-x} nanoparticles for efficient visible light photocatalysts, J. Mater. Chem. A 2 (2014) 4429–4437, https://doi.org/10.1039/C3TA14484D.
[90] T. Montini, V. Gombac, L. Sordelli, J.J. Delgado, X. Chen, G. Adami, P. Fornasiero, Nanostructured Cu/TiO_2 photocatalysts for H_2 production from ethanol and glycerol aqueous solutions, ChemCatChem 3 (2011) 574–577, https://doi.org/10.1002/cctc.201000289.